Diffraction grating parameter retrieval using non-paraxial structured beams in coherent Fourier scatterometry

Soman, S.; Pereira, S. F.; Gawhary, O. El

DOI
10.1088/2040-8986/ac4abb

Publication date
2022

Document Version
Final published version

Published in
Journal of Optics (United Kingdom)

Diffraction grating parameter retrieval using non-paraxial structured beams in coherent Fourier scatterometry

OPEN ACCESS
IOP Publishing
Journal of Optics
J. Opt. **24** (2022) 034006 (9pp)
https://doi.org/10.1088/2040-8986/ac4abb

Diffraction grating parameter retrieval using non-paraxial structured beams in coherent Fourier scatterometry

S Soman*, S F Pereira and O El Gawhary

Optics Research Group, Imaging Physics Department, Faculty of Applied Sciences, Delft University of Technology, Lorentzweg 1, 2628 CJ Delft, The Netherlands

E-mail: s.soman@tudelft.nl

Received 15 November 2021, revised 9 January 2022
Accepted for publication 12 January 2022
Published 3 February 2022

Abstract

In recent years, a lot of works have been published that use parameter retrieval using orbital angular momentum (OAM) beams. Most make use of the OAM of different Laguerre-Gauss modes. However, those specific optical beams are paraxial beams and this limits the regime in which they can be used. In this paper, we report on the first results on retrieving the geometric parameters of a diffraction grating by analysing the corresponding complex-valued (i.e. amplitude and phase) Helmholtz Natural Modes (HNM) spectra containing both the azimuthal (i.e. n) and radial (i.e. m) indices. HNMs are a set of orthogonal, non-paraxial beams with finite energy carrying OAM. We use the coherent Fourier scatterometry (CFS) setup to calculate the field scattered from the diffraction grating. The amplitude and phase contributions of each HNM are then obtained by numerically calculating the overlap integral of the scattered field with the different modes. We show results on the sensitivity of the HNMs to several grating parameters.

Keywords: scatterometry, optical metrology, structured beam, coherent Fourier scatterometry

(Some figures may appear in colour only in the online journal)

1. Introduction

Semiconductor devices have been a major driving force in the rapid technological advances witnessed during the last few decades. The continuous reduction in the size of these devices have made a tremendous impact on our lives both at an individual and societal level. Although the reduction in device size improves the processing speed and lowers the power consumption, it comes at the cost of introducing many manufacturing challenges. With the increasing patterning resolution, determination of the different pattern parameters of nanostructures such as a diffraction grating (period, line-width, height and side wall angles) with sub-nanometer precision becomes one of the key challenges for ensuring a good device performance of a lithographic scanner [1–5].

The fundamental challenge for metrology in manufacturing applications is the inspection of small structures while maintaining good yield and profitability [6]. This limits the use of methods such as Scanning Electron Microscopy and Atomic Force Microscopy as they can be destructive, slow or demanding in terms of operating conditions. Optical scatterometry provides a fast, low cost, precise, and non destructive alternative, making it one of the most prevalent inline metrology techniques in the semiconductor industry. Assuming enough prior knowledge on the sample is available (a condition which is not always met), scatterometry can be considered as a model-based metrology technique based on the light scattered from an object. A unique solution to the inverse scattering problem can be obtained if some information about the object geometry

* Author to whom any correspondence should be addressed.

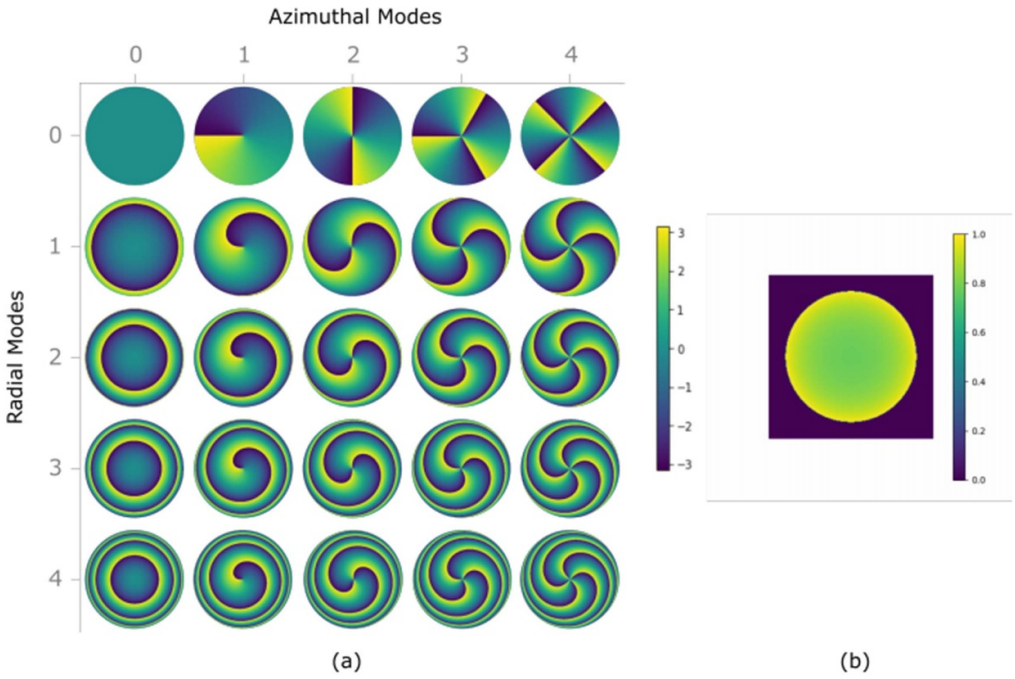

Figure 1. Phase (a) and normalised amplitude (b) profiles of a few HNMs in the Fourier domain. The normalised amplitude profile is the same for all modes.

is known *a priori* [7, 8]. Within the field of scatterometry, there are a number of different measurement strategies that are often used to characterise different symmetric and asymmetric pattern parameters including coherent Fourier scatterometry (CFS), white light interference Fourier scatterometry, spectroscopic ellipsometry, and Mueller polarimetry [9–17].

In CFS, a coherent beam is tightly focused on the sample and the far field patterns are recorded on a CCD camera. These far field maps are compared to rigorous simulations calculated for a range of different grating parameters. Conventional CFS uses truncated Gaussian beams for the coherent illumination of the back focal plane of the objective. Recently, several works have been published demonstrating the use of coherent structured light beams illumination in both CFS [18] and other scatterometric methods [19–25]. Most of them use the Laguerre-Gauss modes, a set of solutions to the paraxial Helmholtz equation, for the illumination. They have the advantage of being shape invariant within the paraxial domain. In this paper, we introduce the use of Helmholtz Natural Modes (HNMs) in CFS to characterise the geometric parameters of a diffraction grating [26]. HNMs are solutions to the Helmholtz equation (and therefore are not limited to the paraxial regime) and make a complete, finite-energy, orthogonal, propagation invariant set of modes. Due to the presence of a helical phase profile, HNMs naturally carry orbital angular momentum (OAM). They also carry a new type of radial topological charge (in the form of a radial phase profile of the angular spectrum of a HNM), that has been shown to play a key role in the so-called spin–orbit coupling for electromagnetic fields [28, 29]. Being a complete and orthogonal basis means that any arbitrary field can be written as a unique expansion of HNMs. While we invite the reader to the reference on the theory of HNMs, here below we briefly recall their basic properties. We will do that by using the scalar theory of optics. For the extension to vectorial electromagnetic fields we refer to El Gawhary *et al* [28]. Let $U(x,y,z)$ be a scalar monochromatic field satisfying the Helmholtz equation and $A^{(0)}(\rho,\phi)$ be its angular spectrum in the Fourier domain in the reference plane $z=0$ with (ρ,ϕ) being the spatial frequencies in the cylindrical coordinates. The expansion of $A^{(0)}(\rho,\phi)$ in HNMs is given as

$$A^{(0)}(\rho,\phi)=\sum_{m,n}C_{m,n}\left[\frac{\exp\left(i2\pi m\lambda\sqrt{\frac{1}{\lambda^2}-\rho^2}\right)}{\left(\frac{1}{\lambda^2}-\rho^2\right)^{1/4}}\exp\left(in\phi\right)\right] \tag{1}$$

where m and n are integers with $m, n=0,\pm1,\pm2,\ldots$ and $C_{m,n}$ are the complex coefficients that define how much each single HNM contribute to making the field $U(x,y,z)$. Each mode is uniquely represented by two integers: the radial index, m, and the azimuthal index, n. The radial index refers to the number of periods contained in the radial phase distribution of each mode. The azimuthal index is equal to the topological charge corresponding to the helical phase distribution of each mode. Throughout the paper, a single HNM is represented using the notation $\mathrm{HNM}_{(m,n)}$ and we have used the terms 'modes' and HNMs synonymously. The amplitude and phase distributions of a few HNMs in the Fourier domain are given in figure 1.

For more details regarding the mathematical properties of the modes, the readers are advised to go through the [26, 27]. The main characteristic which makes these modes appealing for metrology is that the decomposition of a generic field

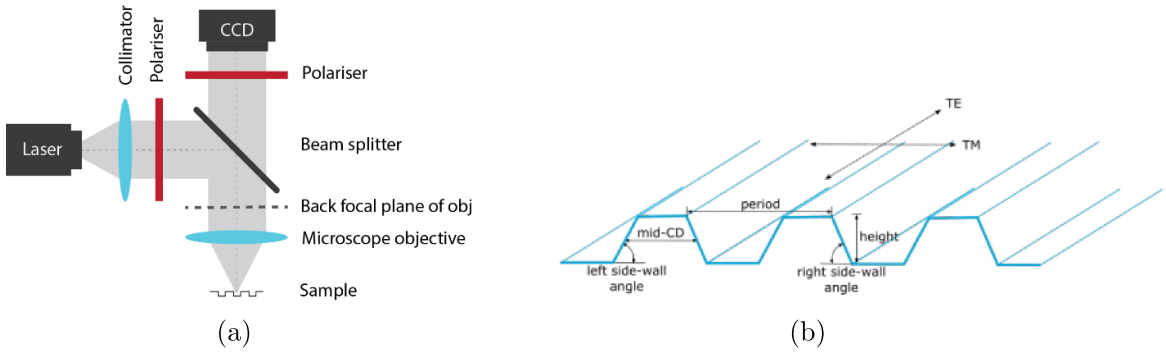

Figure 2. (a) The basics of a coherent Fourier scatterometry setup. The numerical aperture of the objective considered in this work is 0.8. (b) Profile of the diffraction grating used. The trapezoidal profile is parameterised by the period, mid-CD, height, and left and right SWAs of the grating. Transverse Electric (TE) and magnetic TM polarisations represent EM fields at the pupil plane with the electric field parallel and perpendicular to the grating lines respectively.

into HNMs is essentially propagation invariant, in the sense the propagation affects the coefficients $C_{m,n}$ of an expansion in HNMs in the same way, without altering their relative strengths. This property is in stark contrast with other, otherwise very useful bases, like Zernike's polynomials, just to name the most important of them. If free-space propagation does not affect the weights of a decomposition, then any change due to the interaction with an object can be easy to detect and process. In this paper we have tackled, for the first time to the best of our knowledge, the problem of investigating how the interaction with a diffraction grating affects the HNM decomposition of a light probe. More specifically, we have examined the sensitivity of the amplitude and phase distributions for different modes due to variation in the far field maps arising from the changes of different geometrical parameters of the grating, including height, period, mid-CD (critical dimension) and symmetric and asymmetric side wall angles (SWAs) through simulations. In the next section, we briefly introduce the simulation setup followed by the major results and observations.

2. Simulation setup

The simulations of the interaction between the incident field and the 1D-periodic diffraction grating have been done using the rigorous simulation method known as the RCWA (Rigorous Coupled Wave Analysis) [30–33]. Figure 2(a) shows the setup used for the simulations. Light from a laser is coupled to a single mode fiber, collimated and sent to a beam splitter. The light from the beam splitter is focused on the sample using a microscope objective having a numerical aperture of 0.8. The scattered light and spurious reflections are collected by the same focusing lens and the far field distribution is calculated. The distribution represents the total scattered light from all incident angles within the numerical aperture of the objective. The input source wavelength was taken to be 532 nm. For practical considerations input beams with only one polarisation were considered, namely the TM polarisation (polarisation at the pupil plane is perpendicular to the grating lines). The desired output polarisation was obtained using a polariser in front of the detector. The input field had uniform amplitude and constant phase at the back focal plane of the microscope objective. This is often used as a standard input beam and can be used to show the generalisability of using HNMs as a basis for decomposing an arbitrary field. The scatterer considered was a diffraction grating with a trapezoidal profile as shown in figure 2(b). The grating is made of Silicon periodic structures on a Silicon substrate. The refractive index for Silicon was calculated to be $n_{Si} = 4.1360 - i0.010205$ at 532 nm wavelength [34]. Air of refractive index $n_{air} = 1$ was used as the superstrate. Gratings with different periods from 300 to 650 nm, having heights from 100 to 500 nm and mid-CD from 100 nm to 0.9 times the grating period have been simulated. The wavelength and substrate were chosen due to their commonplace usage. The period values were chosen such that the first diffraction order gets captured by the objective lens.

To analyse the change in the amplitude and phase distribution of each mode after scattering, the amplitude and phase of the far field pattern was expanded as a sum of different HNMs. The coefficient corresponding to each mode was obtained by calculating the overlap integral of the scattered field with different modes using the equation,

$$C_{m,n} = \frac{1}{2\pi}\int_0^1\int_0^{2\pi} A^{(0)}(\rho,\phi)\frac{\exp\left(-i2\pi m\lambda\sqrt{\frac{1}{\lambda^2}-\rho^2}\right)}{\left(\frac{1}{\lambda^2}-\rho^2\right)^{1/4}} \times \exp\left(-in\phi\right)\rho\,\mathrm{d}\rho\,\mathrm{d}\phi. \quad (2)$$

3. Results

To investigate the effect of the variation of period on amplitude and phase distribution of the modes, the value of the period of the grating was varied from 300 to 650 nm while keeping the mid-CD and height constant at 200 nm and the left and right SWAs at 90°. In this case, we observe that the phase of certain

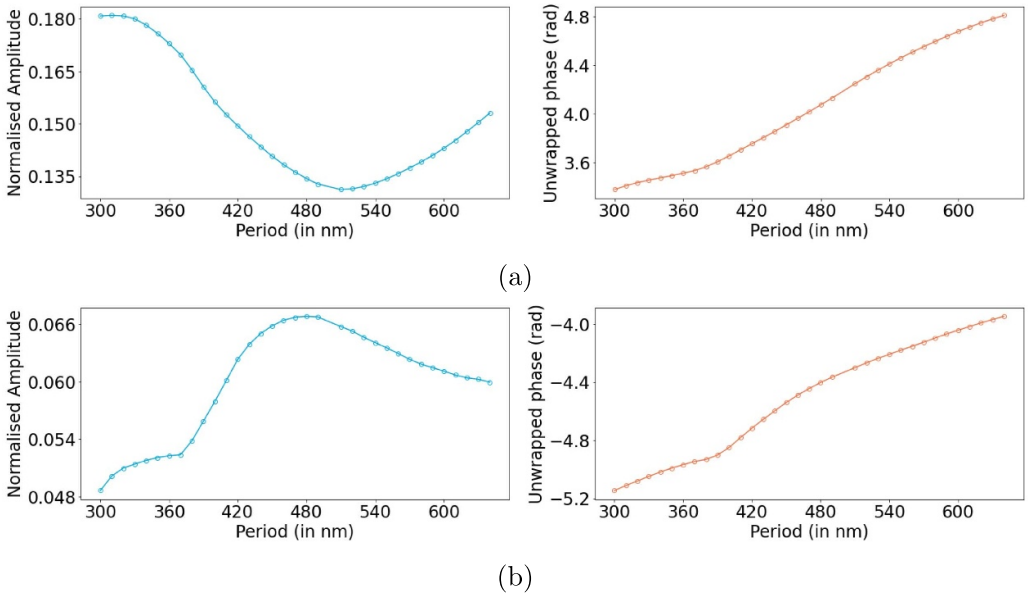

Figure 3. The change in amplitude and phase of (a) (0,0) and (b) (−2,0) modes with respect to variation in period. The height and mid-CD of the grating were kept constant at 200 nm and 200 nm respectively. The amplitude is normalised by the total energy of all the modes.

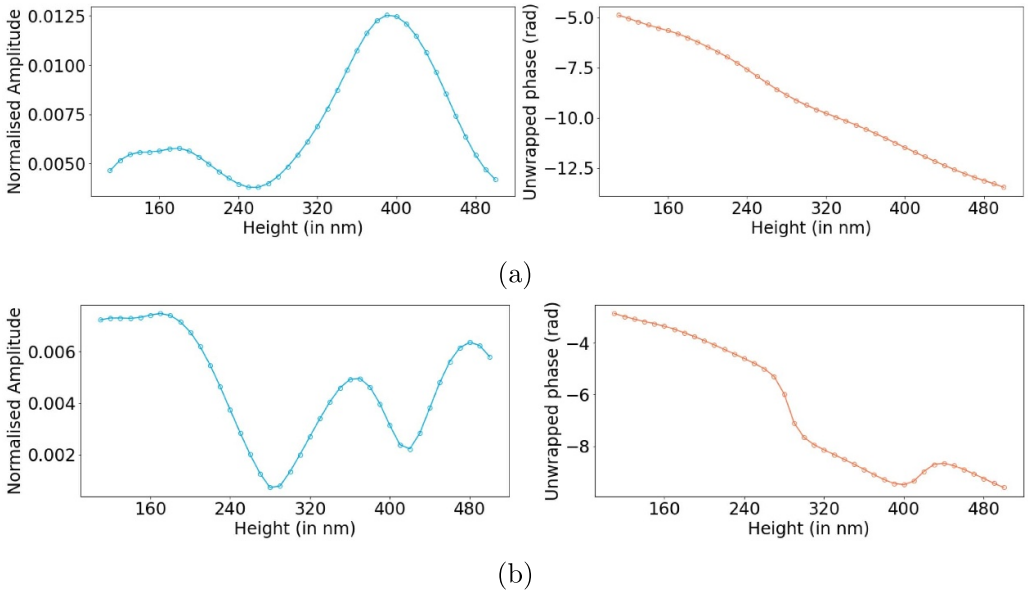

Figure 4. The change in amplitude and phase of the modes (a) (2,4) and (b) (3,4) with respect to variation in height of the grating. The period and mid-CD were kept constant at 410 nm and 210 nm respectively. The phase angles were unwrapped by adding multiples of 2π whenever the jump between consecutive angles were greater than π radians. The amplitude is normalised by the total energy of all the modes.

modes follows a linear relationship with the change in period. Figure 3 shows the amplitude and phase values for the modes (0,0) and (−2,0). As the period increases beyond 332.5 nm, more of the ±1st orders are captured within the numerical aperture. This causes a gradual redistribution of energy from the lower-order HNMs to the higher-order HNMs which can more accurately represent the diffracted field. This is apparent from comparing the amplitude variations of the modes (0,0) to that of (−2,0).

Figure 4 shows the phase and amplitude distributions of the modes (2,4) and (3,4) as the height is increased. The height of the grating was varied from 100 to 500 nm while the period and mid-CD was kept constant at 410 nm and 210 nm, respectively. Similarly, the effect of the mid-CD was studied by

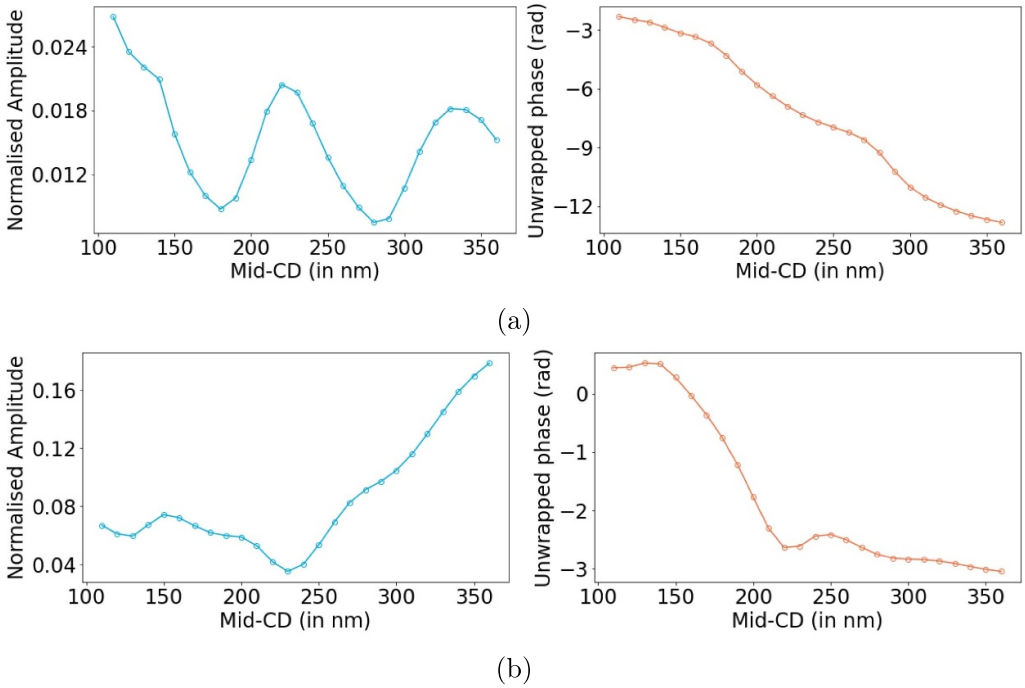

Figure 5. The change in amplitude and phase of the modes (a) (0,2) and (b) (0,0) and with respect to variation in mid-CD. The period and height of the grating were kept constant at 400 nm and 120 nm respectively. The phase angles were unwrapped by adding multiples of 2π whenever the jump between consecutive angles were greater than π radians. The amplitude is normalised by the total energy of all the modes.

simulating different gratings with mid-CD from 100 to 360 nm while the period and height were kept constant at 400 nm and 120 nm respectively. The output of the modes (0,0) and (0,2) are shown in figure 5. The side wall angles in both cases are kept at 90°. We observe that the phase of certain modes decrease monotonically with increase in height and mid-CD. For example, in case of the height parameter, the phase of the mode (2,4) is a linear function of the height while the phase of the mode (3,4), as shown in figure 4(b), is non-unique for different values of height. Figure 5(a), shows the behaviour of the mode (0,2) when the mid-CD is increased. The amplitude of the mode changes in a cyclic manner while the phase of the mode decreases as a monotonous function of mid-CD. Thus, different modes exhibit different behaviour as the different geometric parameters are varied. In some cases the value of the parameter can be obtained using linear regression calculations.

Side wall angles are notorious for being harder to measure compared to other geometric parameters. A change in side wall angles by a few degrees causes only a small change in the total volume of the grating structure. The interaction between the incident field and the scattering object is influenced by the volume of the scattering object. Thus changes in geometric parameters that do not cause a large change in the volume are considerably harder to detect. Figure 6 shows amplitude and phase values for a few HNMs. It is apparent that the phase of the (0,2) mode exhibits a similar linearity as observed in case of the other geometric parameters. The side wall angle retrieval in turn is reduced to an application of a simple linear regression. It is perhaps also interesting to note a sudden dip in the amplitude distributions of the (0,0) and (1,0) modes for side wall angles of 88°. It is surprising that a difference of only 2° causes a sudden change in amplitude. To ensure that this minimum was due to a physical process and not a numerical error, the far field intensity distributions of the gratings with SWAs close to 88° were plotted as shown in figure 7. From the distributions, it seems that near the centre of the 0th order, there is a shift from a local intensity maxima to minima. This was further corroborated by directly calculating the degree of correlation between different intensity distributions. The plot containing the different correlation values is shown in figure 8. The dip in the plot around 88° suggests that the far field pattern from the diffraction grating with side wall angles of 88° becomes quite different compared to the other gratings. Thus, from both a visual inspection of the far field intensity patterns and a quantitative computation of the degree of correlation among them it is evident that the dip in the amplitude spectra of the modes discussed above is real and due to an actual change in the scattered field from different gratings. This analysis confirms that this specific feature was properly picked by decomposition into HNMs.

Another aspect, which is highly relevant in practice, is to see how an analysis of the HNMs spectrum enables us to distinguish cases that are affected by different symmetries. In order to address this case, the HNMs spectra from the

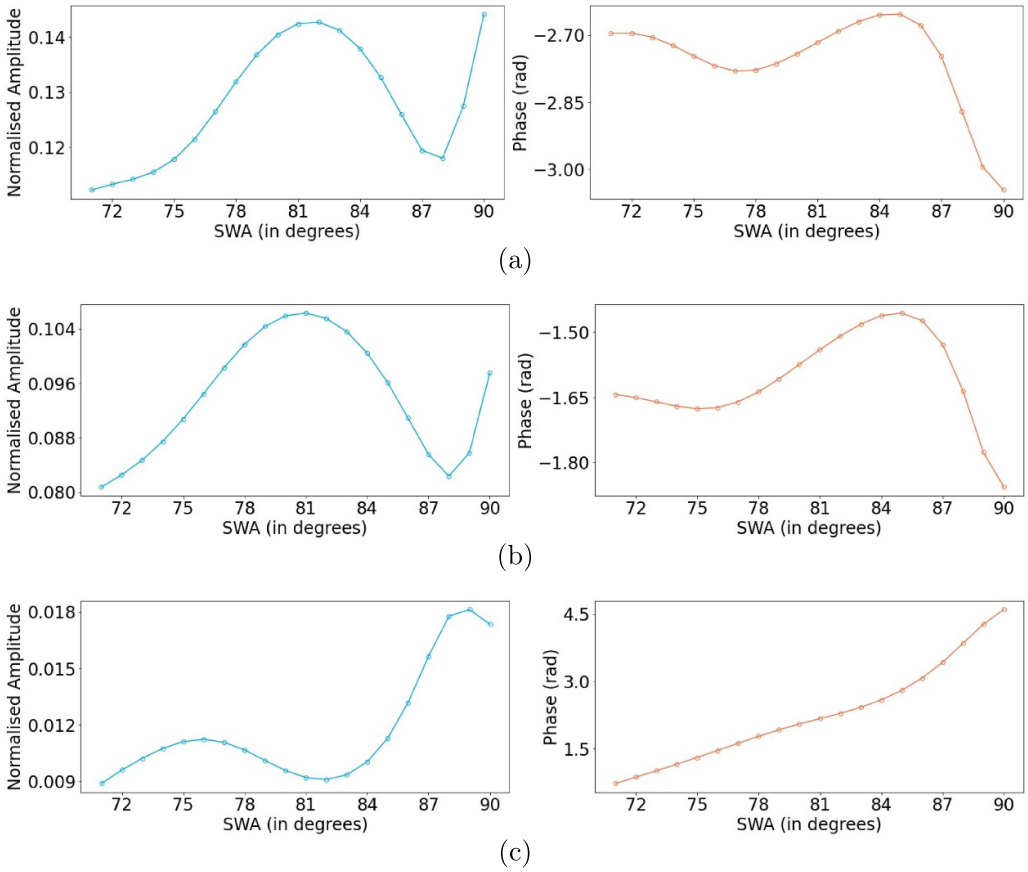

Figure 6. The change in amplitude and phase of the modes (a) (0,0), (b) (1,0) and (c) (0,2) with respect to variation in SWAs. The gratings are symmetric and have the same values for the left and right SWAs. The period, mid-CD and height of the grating were kept constant at 400 nm, 200 nm, and 240 nm respectively. The amplitude is normalised by the total energy of all the modes.

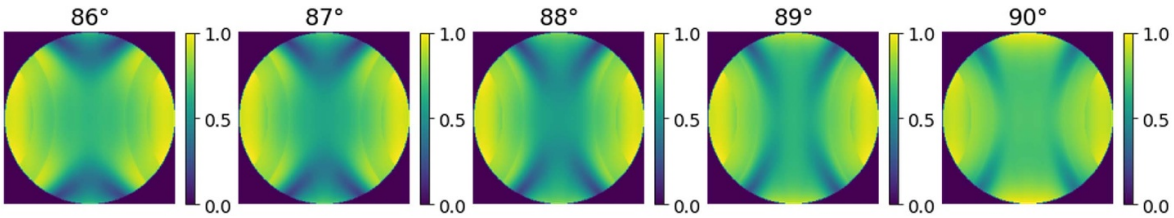

Figure 7. The far field intensity distributions of symmetric gratings when SWAs are varied from 86°–90°. The input and scattered fields have TM polarisation. The period, mid-CD and height of the gratings were kept constant at 400 nm, 200 nm, and 240 nm respectively.

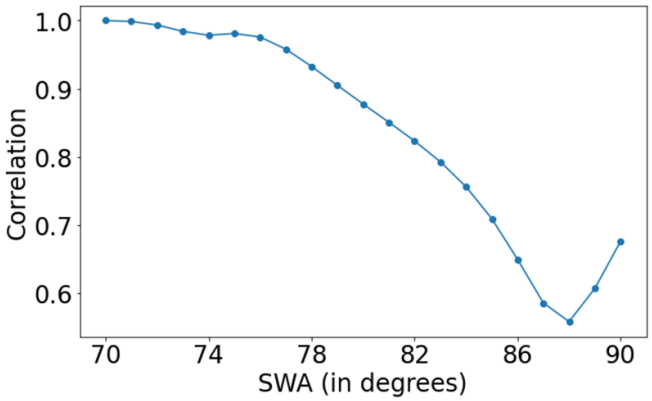

Figure 8. Correlation of the far field intensity distribution on gratings with different SWAs. The input and scattered fields have TM polarisation. The period, mid-CD and height of the gratings were kept constant at 400 nm, 200 nm, and 240 nm respectively.

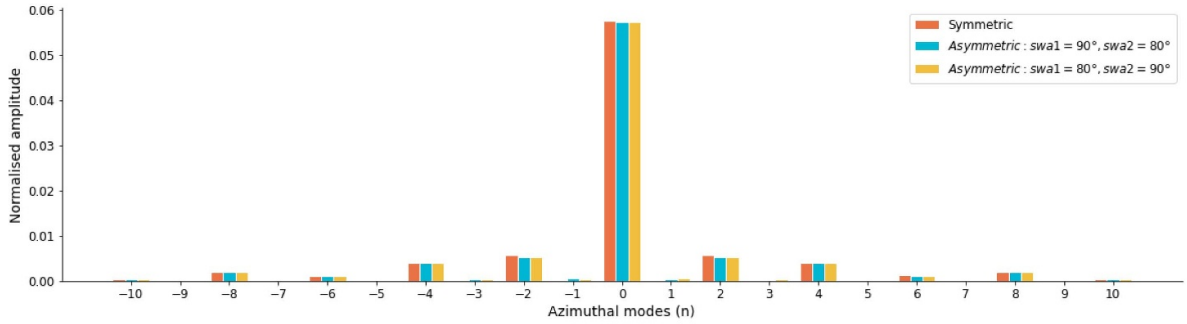

(a) The spectra of the normalised amplitude of azimuthal modes with radial mode $m = 0$.

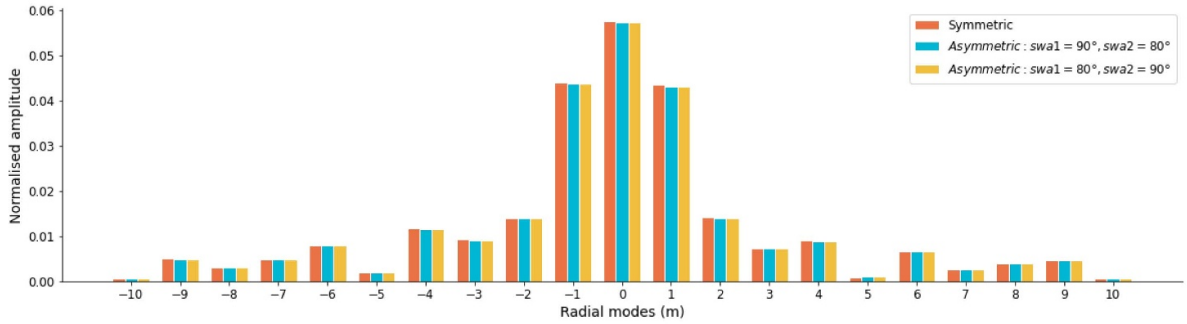

(b) The spectra of the normalised amplitude of radial modes with azimuthal mode $n = 0$.

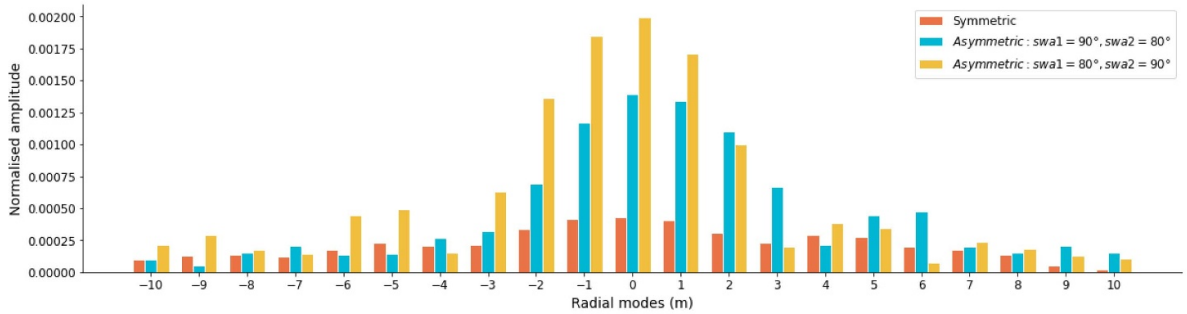

(c) The spectra of the normalised amplitude of radial modes with azimuthal mode $n = 1$.

Figure 9. The amplitude spectra of different HNM obtained from the decomposition of the TM fields scattered from diffraction gratings of period 450 nm, mid-CD 150 nm and height 60 nm with different SWAs. The symmetric grating has both left and right SWAs equal to 90° and the asymmetric gratings has SWA of 80° on the left and 90° on the right or vice versa. The amplitude is normalised by the total energy of all the modes.

decomposition of the fields scattered by symmetric and asymmetric gratings were compared. The symmetric gratings had side wall angles of 90°, identical to each other in both sides of the single line of a gratings line. Asymmetric gratings, in turn, had either a left or right side wall angle of 80° and the other 90°. It is interesting to see how much we can learn about the symmetry of the grating (namely, fully symmetric case, left SWA larger than the right SWA or right SWA larger than the left SWA) by analyzing the corresponding HNMs spectrum. Figure 9 shows the HNM spectra of the far field distribution of the field scattered by a diffraction grating with period 450 nm, mid-CD 150 nm, and height 60 nm. Figure 10 shows a similar plot using a grating of height 100 nm with the other parameters being kept the same. When the grating is shallow the radial modes with even azimuthal index are almost insensitive to asymmetry in SWAs. For deeper gratings, the difference between the amplitudes of the same set of radial modes for symmetric and asymmetric gratings become more apparent. This insensitivity could become a useful tool in situations like overlay measurements where the contributions from the asymmetric SWA is superimposed to the main overlay signal to be detected. In both cases, the amplitude spectra of the modes with odd azimuthal charges seems to be different for all the three gratings, suggesting that the odd modes are sensitive not only to the magnitude of the asymmetry but also to its sign.

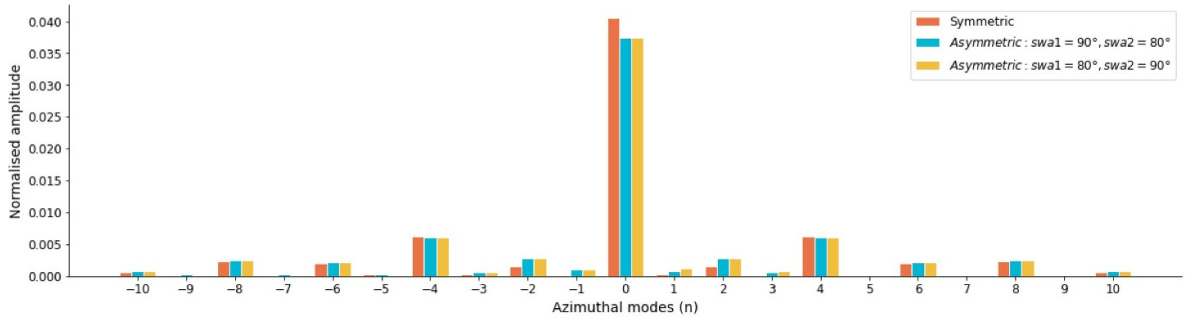

(a) The spectra of the normalised amplitude of azimuthal modes with radial mode $m = 0$.

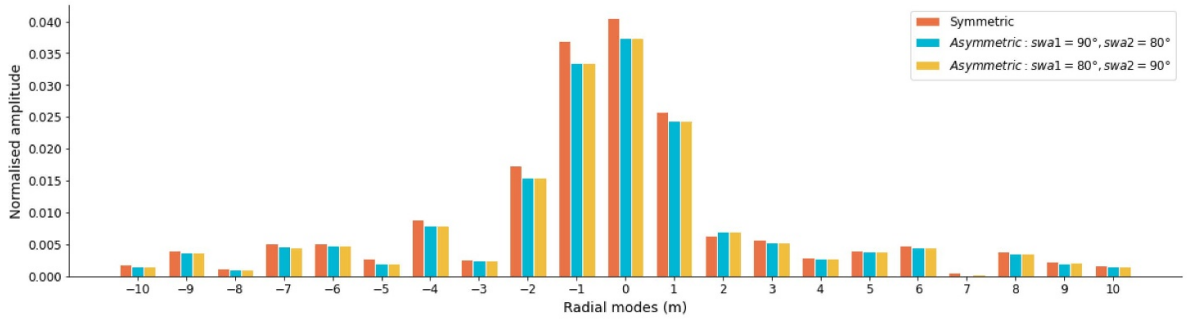

(b) The spectra of the normalised amplitude of radial modes with azimuthal mode $n = 0$.

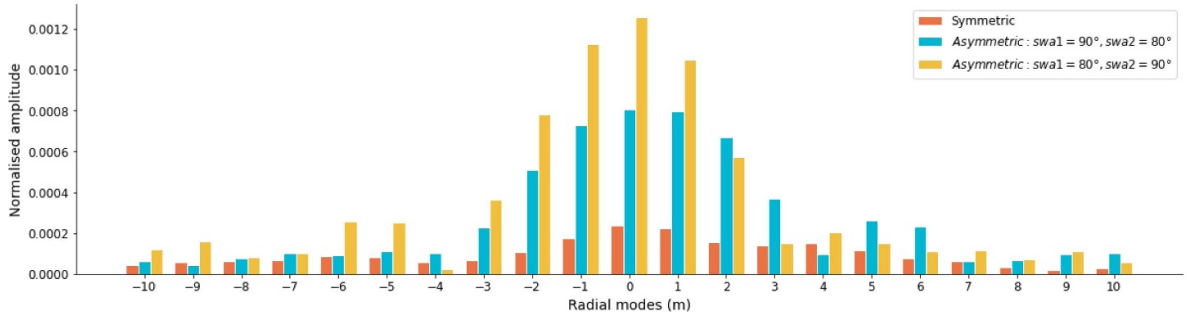

(c) The spectra of the normalised amplitude of radial modes with azimuthal mode $n = 1$.

Figure 10. The amplitude spectra of different HNMs obtained from the decomposition of the TM fields scattered from diffraction gratings of period 450 nm, mid-CD 150 nm and height 100 nm with different SWAs. The symmetric grating has both left and right SWAs equal to 90° and the asymmetric gratings have SWAs with 80° on one side and 90° on the other.

4. Discussion

The goal of this work has been to show how the geometric information of a diffraction grating is encoded into the weights of the expansion in HNMs of the scattered field in a coherent Fourier scatterometry configuration. This was done by analyzing the complex-valued HNM spectra containing both the radial (i.e. m) and azimuthal (i.e. n) indices. The rigorous electromagnetic simulations done show that the phase of specific HNMs have a linear relationship with the different geometric parameters whose values can then be obtained directly using linear regression calculations. The even azimuthal mode spectra for shallow gratings is insensitive to the asymmetry of the grating. The odd azimuthal modes, on the other hand can be used to detect both magnitude and sign of the asymmetry. In experimental conditions, once the phase and amplitude of the fields are known [35], one could follow our method and determine the expansion in HNMs. However, in order to compare experiment with the simulations, more work should be done in considering the noise and other experimental imperfections in the simulations.

Data availability statement

The data that support the findings of this study are available upon reasonable request from the authors.

Acknowledgments

Omar El Gawhary and Silvania F Pereira acknowledge Project 17FUN01 'BeCOMe' within the programme EMPIR. The EMPIR initiative is co-founded by the European Union's

Horizon 2020 research and innovation programme and the EMPIR Participating Countries.

ORCID iD

S Soman https://orcid.org/0000-0002-8316-8639

References

[1] Mack C 2007 *Fundamental Principles of Optical Lithography* (New York: Wiley)
[2] Raymond C J, Murnane M R, Prins S L, Sohail S, Naqvi H and McNeil J R 1997 *J. Vac. Sci. Technol.* B **15** 361
[3] Edwards C, Arbabi A, Popescu G and Goddard L L 2012 *Light Sci. Appl.* **1** e30
[4] Wurm M, Bonifer S, Bodermann B and Richter J 2011 *Meas. Sci. Technol.* **22** 094024
[5] Muthinti R, Loubet N, Chao R, Ott J and Guillorn M *et al* 2016 *Proc. SPIE* **9778** 977810
[6] International Roadmap for Devices and Systems Metrology 2021 (available at: https://irds.ieee.org/edns/2021/metrology)
[7] Naqvi S S H, Krukar R H, McNeil J R, Franke J E, Niemczyk T M, Haaland D M, Gottscho R A and Kornblit A 1994 *J. Opt. Soc. Am.* A **11** 2485–93
[8] Endres J, Diener A, Wurm M and Bodermann B 2014 *Meas. Sci. Technol.* **25** 044004
[9] Kumar N, Petrik P, Ramanandan G K P, El Gawhary O, Roy S, Pereira S F, Coene W M J and Urbach H P 2014 *Opt. Express* **22** 24678–88
[10] Ferreras Paz V, Peterhänsel S, Frenner K and Osten W 2012 *Light Sci. Appl.* **1** e36
[11] Huang H T and Terry J F L 2004 *Thin Solid Films* **455–456** 828–36
[12] Novikova T, De Martino A, Hatit S B and Drévillon B 2006 *Appl. Opt.* **45** 3688–97
[13] Raymond C 2005 *AIP Conf. Proc.* **788** 394–402
[14] Roy S, Pereira S F, Urbach H P, Wei X and El Gawhary O 2017 *Phys. Rev.* A **96** 013814
[15] Roy S, El Gawhary O, Kumar N, Pereira S F and Urbach H P 2012 *J. Eur. Opt. Soc. Rapid Publ.* **7** 12031
[16] Kumar N, El Gawhary O, Roy S, Pereira S E and Urbach H P 2013 *J. Eur. Opt. Soc. Rapid Publ.* **8** 13048
[17] El Gawhary O and Petra S 2014 Method and apparatus for determining structure parameters of microstructures *Patent No.* TW 1464366
[18] Wang B, Tanksalvala M, Zhang Z, Esashi Y, Jenkins N W, Murnane M M, Kapteyn H C and Liao C T 2021 *Opt. Express* **29** 3342–58
[19] Peterhänsel S, Gödecke M L, Ferreras Paz V, Frenner K and Osten W 2015 *Opt. Express* **23** 24246–56
[20] Hermosa N, Rosales-Guzmán C, Pereira S F and Torres J P 2014 *Opt. Lett.* **39** 299–302
[21] Torner L, Torres J P and Carrasco S 2005 *Opt. Express* **13** 873–81
[22] Molina-Terriza G, Rebane L, Torres J P, Torner L and Carrasco S 2007 *J. Eur. Opt. Soc.* **2** 07014
[23] Cisotto L, Zhu Y, Pereira S F and Urbach H P 2015 Spatial mode projection for side-wall angle measurements *Proc. SPIE Munich, Germany* **9526** 952607
[24] Faridian A, Ferreras Paz V, Frenner K, Pedrini G, den Boef A and Osten W 2015 *J. Micro/ Nanolithogr. MEMS MOEMS* **14** 021104
[25] Gödecke M L, Peterhänsel S, Buchta D, Frenner K and Osten W 2017 *Proc. SPIE* **10449** 104490C
[26] El Gawhary O 2017 *New J. Phys.* **19** 013021
[27] El Gawhary O 2015 *Opt. Lett.* **40** 2626–9
[28] El Gawhary O, van Mechelen T and Urbach H P 2018 *Phys. Rev. Lett.* **121** 123202
[29] El Gawhary O, van Mechelen T and Urbach H P 2019 *Phys. Rev. Lett.* **122** 089302
[30] Moharam M G and Gaylord T K 1981 *J. Opt. Soc. Am.* **71** 811–8
[31] Li L 1996 *J. Opt. Soc. Am.* A **13** 1870–6
[32] van Kraaij M and Maubach J 2004 *Progress in Industrial Mathematics at ECMI* **8** 164–8
[33] Popov E and Neviere M 2000 *J. Opt. Soc. Am.* A **17** 1773–84
[34] Vuye G, Fisson S, Nguyen Van V, Wang Y, Rivory J and Abelés F 1993 *Thin Solid Films* **233** 166–70
[35] Kumar N, Cisotto L, Roy S, Ramanandan G K P, Pereira S F and Urbach H P 2016 *Appl. Opt.* **55** 4408–13